Mineralogy and Petrology (2024) 118:41–54
https://doi.org/10.1007/s00710-023-00842-1

RESEARCH

Mineral-scale insights into the petrogenesis of the 3.30 Ga rhyolite in the Contendas-Mirante region, northern São Francisco Craton, Brazil: implications from results of plagioclase and biotite analyses

Eliana M. Branches Farias[1] · Cristiano C. Lana[1] · Stefano A. Zincone[1] · Glaucia N. Queiroga[1] · Leonardo M. Graça[1]

Received: 2 February 2023 / Accepted: 5 July 2023 / Published online: 4 August 2023

Abstract
The 3.30 Ga high-silica volcanic system of the Gavião Block, São Francisco Craton, represents the remnants of within-plate magmatism related to an intracontinental rift. However, the petrogenetic processes that may have taken place in the relatively shallow primitive continental crust has not been fully constrained due to a scarce record. Petrographic and chemical analyses in biotite, as well as in-situ Sr isotope ratios in plagioclase, were used to trace petrogenetic processes and physicochemical conditions of the magmatic system. The subvolcanic rock has a well-preserved primary volcanic feature represented by magma flow textures, euhedral to subhedral plagioclases, rapakivi microstructures, and glomerocrysts. Plagioclase populations formed at two distinct stages recorded by trace elements and Sr isotope. Plagioclase phenocrysts and rapakivi phenocrysts have a slight enrichment of light rare earth elements (LREE), Sr/Ba ratio, and slight variation of Sr isotopes composition. Meanwhile, other phenocrysts and rapakivi crystals have low LREE, Sr/Ba, and a limited variation of Sr isotope ratio. Mineral chemistry evidence points to country rock assimilation during plagioclase formation and a crustal source for primary biotites under oxidized conditions.

Keywords Rhyolite · Paleoarchean · Chemical signature · Plagioclase · Sr isotope · Biotite

Introduction

The 3.30 Ga high-silica rhyolites of the Gavião Block are unusual metaluminous to peraluminous ferroan calcic rocks formed in an intracontinental tectonic setting after the formation and stabilization of new continental crust (Zincone et al. 2016). These rhyolites, according to Zincone et al. (2016), are the products during the first stage of rifting and continental break-up. The Paleoarchean age of the rhyolites, combined with their well-preserved primary petrographic features, make them an excellent natural case of study for investigating tectono-magmatic processes in the early Earth. These rocks are not associated with mafic to intermediate units as other Paleoarchean felsic rocks interlayered with basaltic to komatiitic flows in eastern Pilbara and Barberton, South Africa (e.g. Champion and Smithies 2007; Kröner et al. 2013; Smithies et al. 2019). Instead, they are associated with granitic intrusions like Boa Sorte and Meiras granite of similar trace element compositions and ages (Zincone et al. 2016), providing an inter-related plutonic-volcanic system at a key time in the Earth's history.

Throughout the Archean, felsic rocks acquired increasingly complex geochemical signature during petrogenetic processes, including partial melting of pre-existing continental crust, interactions between mantle peridotite and incompatible element-rich components and melting of meta-igneous older lithologies via anatexis (Laurent et al. 2014). Although Paleoarchean felsic volcanism is not significantly investigated worldwide, a few studies have demonstrated its important role in primitive crustal thickening associated with internal reworking (Agangi et al. 2018). For example, the felsic volcanism in the Pilbara Craton, located at Western Australia, reveals the interaction of magma differentiation and crustal contamination in the formation of protocontinent (Smithies et al. 2019).

Editorial handling: C. Wang

✉ Eliana M. Branches Farias
embfarias@gmail.com

[1] Programa de Pós-Graduação em Evolução Crustal e Recursos Naturais, Departamento de Geologia, Escola de Minas, Universidade Federal de Ouro Preto, Morro do Cruzeiro, Ouro Preto 35400-000, MG, Brazil

In Archean terrains, few Paleoarchean outcrops of felsic magmatism have preserved primary minerals assemblages (e.g. Champion and Smithies 2007; Huston et al. 2007; Agangi et al. 2018; Condie 2019). The São Francisco Craton is an outstanding example with a well-preserved Archean crustal segment which can help to constrain igneous processes and provide clues to the magmatic system evolution (Martin et al. 2005; Zincone et al. 2016; Zincone and Oliveira 2017; dos Santos et al. 2022; Gordilho Barbosa et al. 2022). In-situ analysis of key minerals, such as plagioclase and biotite, which are known to preserve robust isotope, major, and trace element signatures, ensures confidence in what is being analyzed. Isotope studies provide detailed information of magmatic evolution that is challenging to reconstruct using bulk rock compositions (Kemp et al. 2007).

Plagioclase mineral chemistry and Sr isotope analyses may elucidate the processes that occurred during magma cooling (e.g. Tepley and Davidson 2003; Wolff et al. 2011; Chen et al. 2015; Gao et al. 2015), while the use of biotite can trace changes in physicochemical conditions and the nature of the parental magma (e.g. Abdel-Rahman and Abdel Fattah 1994), making these minerals useful tools for investigating igneous systems. The combination of mineral scale examination with petrography may be outstanding instruments for investigating crystallization processes such as assimilation, contamination, magma mixing, and mingling with magma sources. Plagioclase and biotite are two important minerals for investigating igneous systems. For these reasons, they were chosen to constrain the physicochemical composition of Contendas rhyolite during its formation. In this article, we evaluated petrographic textures, mineral chemistry, and plagioclase Sr isotopic signatures of the rhyolite to better understand the magma composition, its physicochemical conditions, and oxygen fugacity (fO_2) during crystallization.

Geological context

The São Francisco Craton is one of the largest in South America, containing the ancient gneiss complexes dated at 3.60–3.64 Ga (Oliveira et al. 2020). The Archean rocks crop out in the northern (Bahia State) and southern (Minas Gerais State) portions of the craton (Teixeira et al. 2017). In the northern portion of the São Francisco Craton, the basement is represented by the Archean terranes of Gavião, Serrinha, Jequié, and Itabuna-Salvador-Curaçá blocks (Barbosa et al. 2003; Barbosa and Sabaté 2004). The Gavião Block is the oldest Archean nuclei in the São Francisco Craton comprising tonalite-trondhjemite-granodiorite (TTG) gneisses, greenstone belts, metavolcano-sedimentary sequences, and several granitic plutons (Nutman and Cordani 1993; Martin et al. 1997; Santos-Pinto et al. 2012; Zincone et al. 2016; dos Santos et al. 2022; Gordilho Barbosa et al. 2022; Fig. 1).

The southern Gavião Block is limited to the east by the Paleoproterozoic Contendas-Jacobina Lineament (Sabaté et al. 1990). Geochronologic constraints protract the São Francisco Craton from Paleoarchean and Neoarchean (Teixeira et al. 2017), demonstrating a crustal evolution akin to the Kaapvaal-Zimbabwe and Pilbara cratons, particularly before 3.0 Ga (Gordilho Barbosa et al. 2022). The geologic evolution of the northern and southern portions of the Gavião Block indicates Eo-to-Paleoarchean crustal growth, as evidenced by TTG magmatism and partial melting of Eoarchean crust, with a minor contribution from a mantle source (Martin et al. 1997; Gordilho Barbosa et al. 2022). The 3.30 Ga high-silica volcanism is found in the northern and southern parts of the block and is associated with intraplate magmatism and intracrustal differentiation processes (Zincone et al. 2016).

The 3.30 Ga high-silica rhyolites of Contendas and Mundo Novo are found 200 km apart from each other (Zincone et al. 2016). They occur inliers within the Mundo Novo and Contendas-Mirante greenstone belts, but contacts between the rhyolites and gneisses or metasedimentary rocks are not observed in the field (Marinho et al. 1993a; Zincone et al. 2016). These volcanic rocks are also unrelated to any other meta-volcanic unit, indicating lower greenschist facies metamorphism (Zincone et al. 2016). The Contendas rhyolite, according to Zincone et al. (2016), represents the high-silica magmatism of the southern of the block formed in the early stages of rifting and continental break-up. Intracontinetal rifting may have occurred coeval with or following the high-silica intraplate magmatism and the Au-U-bearing Jacobina Basin siliciclastic sequence, in the northern of the block (Mascarenhas et al. 1998; Teles et al. 2015; Zincone and Oliveira 2017).

The 3.30 Ga high-silica plutonic-volcanic system were formed after TTG magmatism and stabilization of the Gavião lithosphere indicated by high-K magmatism (Zincone et al. 2016). Paleomagnetic research findings on the Contendas rhyolite revealed an eastward sub-vertical coherent lava flow direction preserved during its formation (Amaral 2021).

The Gavião Block rhyolites are unusual for a number of reasons (Zincone et al. 2016): (1) they are unusually high in silica (74–79 wt%); (2) they formed at very high temperature (915 – 820 °C); (3) the chemistry ranges from ferroan calcic metaluminous to peraluminous; (4) primary features are common, including flow textures, and euhedral phenocrysts of plagioclase (Zincone et al. 2016). These rocks also have a homogeneous trace element pattern and a heterogeneous zircon Hf isotope. The whole-rock geochemistry shows negative anomalies in Nb-Ta, Sr, and Ti, followed by relatively fractionated LREE, resembling the geochemical signature of continental arc magmas (Zincone et al. 2016).

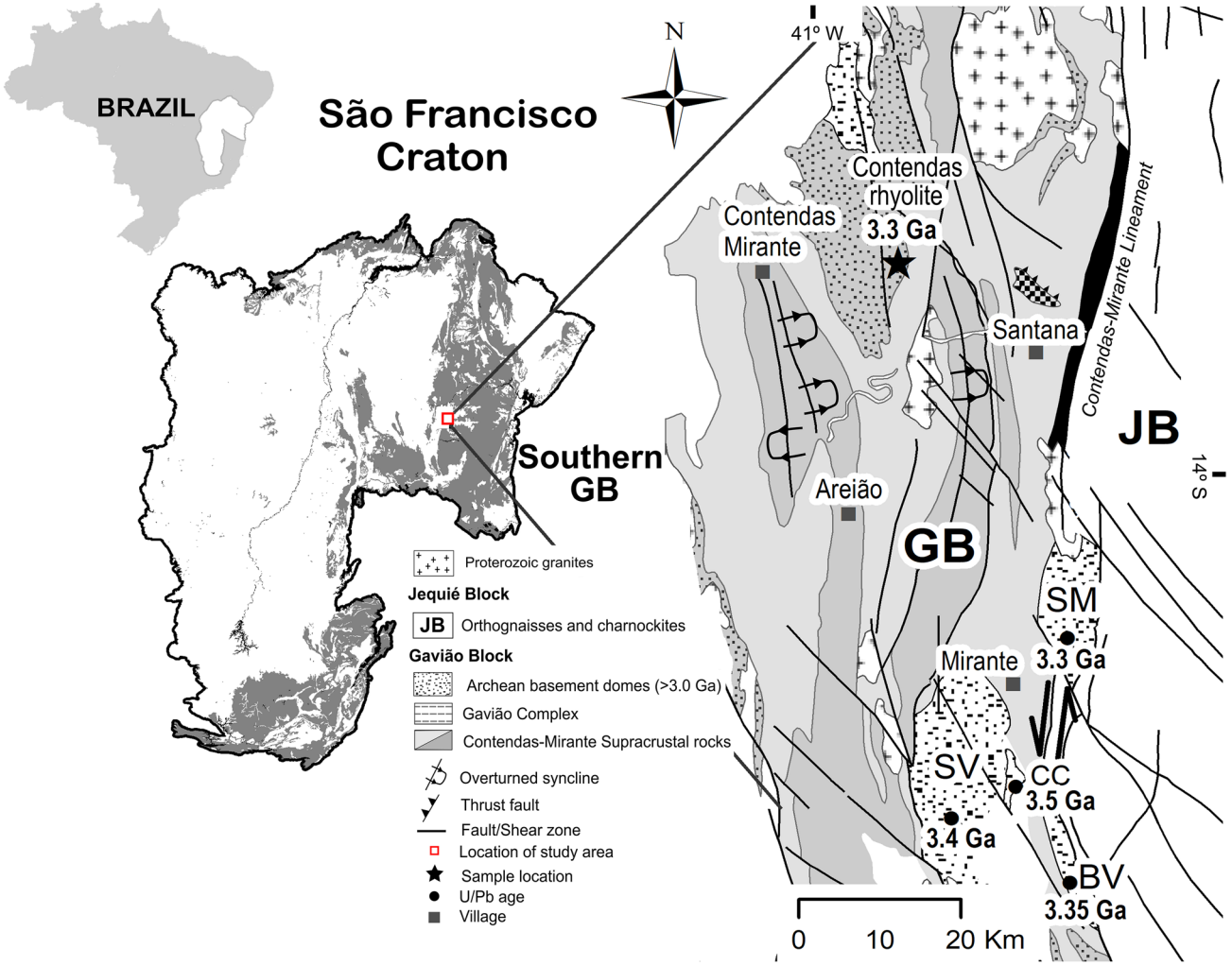

Fig. 1 Geologic map showing the location of Contendas rhyolite samples, represented by a star in the northern of São Francisco Craton (modified after Marinho et al. 1993a, b). The abbreviations are: GB - Gavião Block; JB - Jequié Block; SV - Sete Voltas dome; SM - Serra dos Meiras dome; BV - Boa Vista/Mata Verde dome; CC - Caldeirão Complex

The Hf isotopes show large range of $\varepsilon Hf_{(t)}$ (0 to -7) and older model ages ($T_{DM,}$ where DM means depleted mantle) of 3.54–3.88 Ga and up to 4.02 Ga (Zincone et al. 2016). Such sub-volcanic rocks would have been interpreted to be generated from extraction and emplacing of highly silicic residual liquid formed by crystallization of granitic magma in a relatively shallow (< 10 km) reservoir, now represented by the granite massifs (Zincone et al. 2016).

Materials and methods

Samples

Four samples of Contendas rhyolite were used in this study for petrographic analysis, biotite and plagioclase mineral chemistry, and in-situ Sr isotope analysis on plagioclase. These samples are from the southern part of the Gavião Block. They were collected from distinct incidences within the same outcrop, making it difficult to differentiate contact relationships with other lithologies. They were collected at the location with coordinates 13°40'11"S and 40°54'22"W, and were designated as TZD-31 A, TZD-31 C, TZD-31D, and TZD-31E.

The 3.30 Ga high-silica rhyolite (Zincone et al. 2016) has a porphyritic texture with quartz and feldspar crystals larger than 1 mm size. Phenocrystals are embedded in fine-grained matrix that mainly consists of quartz, feldspars, and biotite minerals, with traces of chlorite and magnetite.

Major elements

Feldspars were investigated using the system electron probe micro-analyser (EPMA). A total of 156 individual measurements were taken from 34 crystals. EPMA chemical analysis

was also used to analyse biotite composition, with 49 individual measurements from 21 crystals. Major element analyses of plagioclase and biotite were performed at Microscopy and Microanalysis Laboratory, using a JEOL JXA-8230 EPMA system with five wavelength dispersive spectrometers (WDS) coupled with one Oxford EDS detector. The analytical conditions were 15 kV accelerating voltage, 10nA beam current and spot size of 5 µm in plagioclase and biotite. The reference materials used were anorthoclase for Na, fluorite for F, quartz for Si, corundum for Al, olivine for Mg, barite for Ba, magnetite for Fe, scapolite for Cl, chromite for Cr, strontianite for Sr, fluorapatite for P, ilmenite for Ti, fluorapatite for Ca, microcline for K and MnO_2 for Mn. ZAF matrix corrections were applied and total iron content was taken as FeO. Counting times on peak and background were 10/5 s for all elements (Na, F, Si, Al, Mg, Fe, Cl, Cr, P, Ti, Ca, K, Mn) except for Ba and Sr (30/15 s).

Trace elements

The trace elements content of feldspars was obtained from 31 spots on 14 selected feldspar crystals. The trace element analyses were carried out at Isotopic Geochemistry Laboratory, by laser ablation-quadrupole-inductively coupled plasma-mass spectrometry (LA-Q-ICP-MS) Agilent 7700x coupled with New Wave Research UP-213 (NdYAG 213). The working conditions were 10 Hz of frequency and 50 µm of size spot. Helium gas was used as conductor and then mixed with argon in the ablation cells. Si was used as the internal standard for correction of inter-element fractionation. External standards such as NIST-610, BCR-2 and BHVO were used for signal correction. GLITTER software (Griffin et al. 2008) was used to refine the final data.

In-situ Sr isotopes

In-situ Sr isotope analyses were carried out on 11 feldspar crystals in a total of 25 measurements. Plagioclase crystals were chosen based on the major populations observed in the petrography described in the following sections. The point analyses aim for core-rim of plagioclase phenocrysts and rims of rapakivi crystals for in-situ Sr isotope determination. The alternative analyses on solely rapakivi rims were due to the core's K-feldspar composition. Sr isotope composition was performed by Thermo Scientific Neptune Plus Multi-collector MC-ICP-MS coupled with laser ablation device 193 nm HelEX Photon Machine in the Isotopic Geochemistry Laboratory. Plagioclase crystals from the Contendas rhyolite were measured in spots of 50 µm (samples TZD-31 C; -31D; 31-E). Working conditions were 10 Hz for ablation frequency and 6 J/cm^2 for energy density. The ablated material was carried into the ICP using helium gas. The laser ablation measurement was 60s long and the blank gas of Kr took was 30s for measuring. The correction for ^{84}Kr to ^{84}Sr and ^{86}Sr interference was performed by subtracting the background from the signal intensity. The interference of ^{87}Rb on ^{87}Sr was corrected by the ^{85}Rb/^{87}Rb ratio exponential law. Repeated measurements of international and internal standards such as calcite standard MIR (reference material), coral, Madagascar apatite and BHVO-2 confirmed the accuracy of the ^{87}Sr/^{86}Sr ratio. Further detail on the methods of ICP-MS can be found in Wilson (1997) and Yang et al. (2011).

Thermobarometer for volcanic systems

Plagioclase- and alkali feldspar-liquid thermobarometers of Putirka (2008) were applied to plagioclase crystals to estimate temperature and pressure during crystallization. Equation 24a and 25a of Putirka (2008) were used. The whole rock composition of Zincone et al. (2016) was used as the 'liquid' composition, and the microanalysis data of this research were used for feldspars compositions. The K_D(Ab-An) equilibrium test was used to validate the results by determining the equilibrium conditions between crystal and melt.

Results

Petrography and mineral chemistry

The Contendas rhyolite has a porphyritic texture characterized by coarse-grained plagioclase and K-feldspar phenocrysts with tabular shapes and coarse rounded quartz grains presenting undulose extinction embedded in a fine-grained groundmass of quartz, orthoclase, albite, biotite, and chlorite. Some quartz grains are fine-grained, being part of the matrix. Zircon and magnetite are important accessories, whereas chlorite, carbonate, sericite, and epidote are present as secondary minerals.

Feldspar phenocrysts can be found in the microcrystalline matrix as tabular individual crystals and glomerocrysts with planar and irregular contacts (Fig. 2a). Plagioclase grains are characterized by the presence of albite and polysynthetic twining in the groundmass. Rapakivi microstructure is another igneous texture found in the rhyolite and occurs tabular and subhedral feldspars, characterized mainly by a K-feldspar core and a plagioclase rim (Fig. 2b). Small feldspars crystals are also surrounded by mica (Fig. 2c). This microstructure is found both in individual feldspars and also in aggregates (Fig. 2d). All crystals that characterize the studied samples are clearly oriented in the felsic groundmass (Fig. 2e).

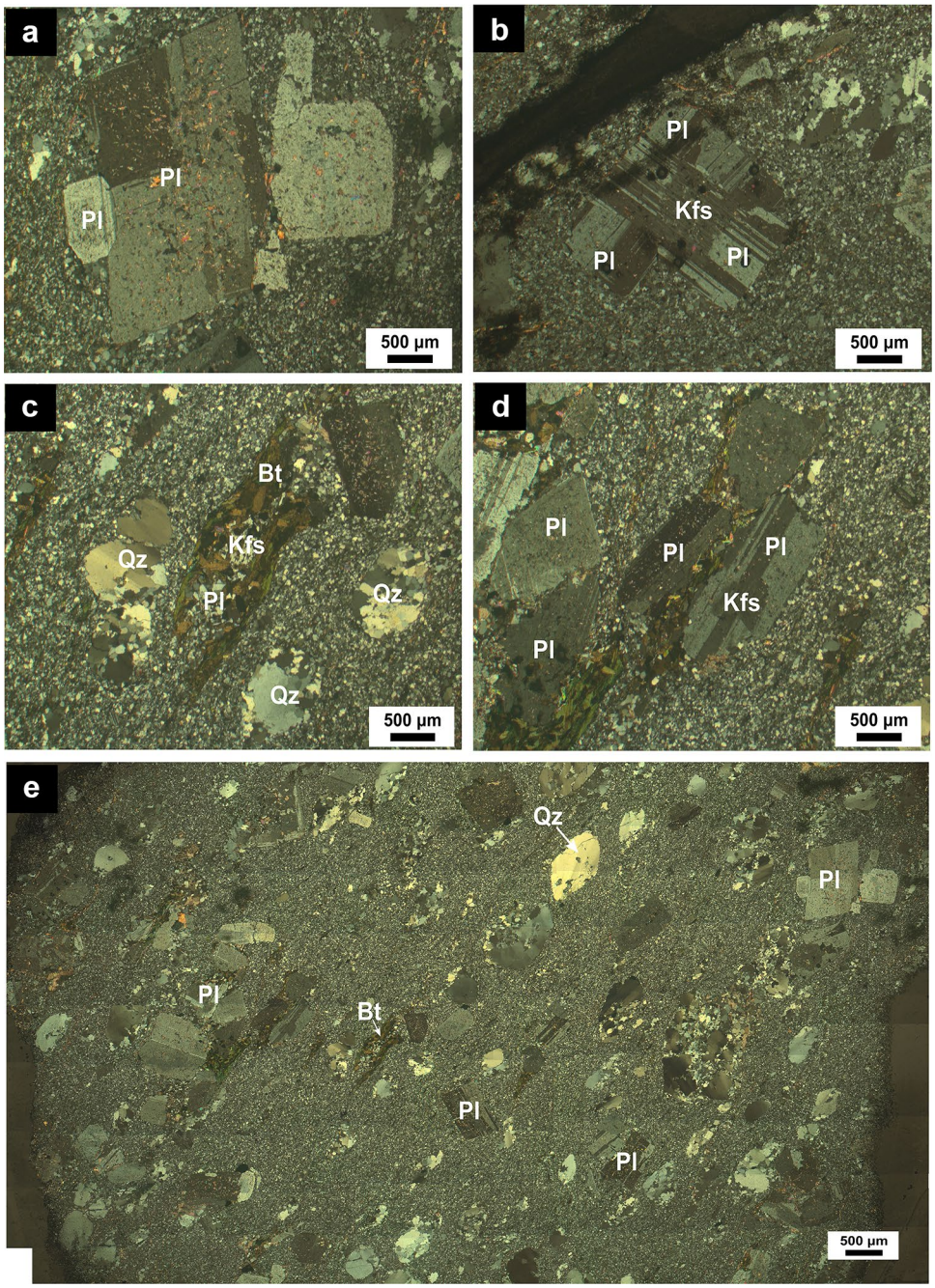

Fig. 2 Cross-polarised transmitted-light photomicrographs. **a** Plagioclase phenocrysts embedded in a fine-grained matrix. **b** Plagioclase phenocryst with rapakivi-like microstructure showing K-feldspar core and plagioclase rim. **c** Microphenocrysts enveloped in biotite. **d** Aggregate of subhedral and anhedral feldspars and rapakivi-like microstructure. **e** Microscope view of TZD-31E thin section showing phenocryst orientation. Minerals abbreviations are: Pl - plagioclase; Qz - quartz; Kfs - K-feldspar; Bt - biotite, according to Whitney and Evans (2010)

Plagioclase

Plagioclase crystals in the Contendas rhyolite are divided into three populations: phenocrysts (500–2300 µm), rapakivi (1400–2300 µm), and microphenocrysts enveloped in biotite (100–150 µm) (Fig. 2a–f). Meanwhile, the rhyolitic groundmass of quartz, plagioclase, K-feldspar, biotite, magnetite, and tiny flakes of chlorite, are fine-grained (< 50 µm). Plagioclase phenocrysts are euhedral to subhedral with tabular shapes. Rapakivi crystals are phenocrysts, euhedral to subhedral, characterized by K-feldspar cores and plagioclase rims. Both plagioclase crystals are commonly found as glomeroporphyritic aggregates in the felsic groundmass. Plagioclase and K-feldspar microphenocrysts are enveloped in biotite showing zircon inclusions and opaque minerals such as magnetite. Plagioclase populations have been moderately altered to white mica and locally calcite.

The major compositional variation in the three types is small, with albite composition (Fig. 3a, b). Results are available in Tables S1 and S3 in the electronic supplementary material (ESM). The phenocrysts have Ab_{96-98}, total iron (FeO_T) ≤ 0.13 wt% and MgO ≤ 0.02 wt%. Sr and Ba contents

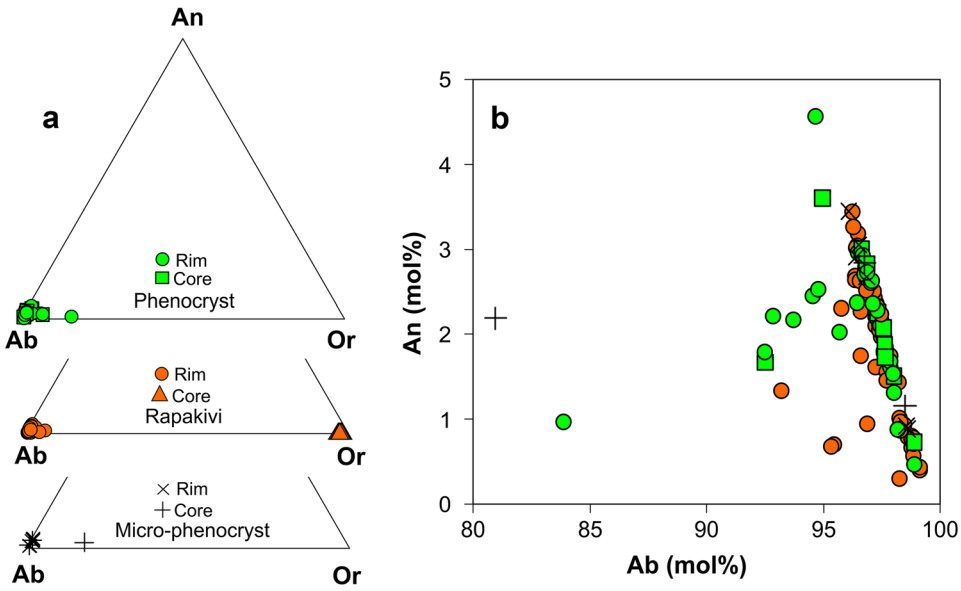

Fig. 3 Composition variation of plagioclase crystals from Contendas rhyolite. **a** Ternary diagram of plagioclase populations. **b** An versus Ab plot, showing the variations of Na and Ca in plagioclase. Mineral abbreviations are: An - anorthite; Or – orthoclase; Ab - albite

vary between 117 and 310 and 3-662 ppm, respectively. Rapakivi crystals have rims of Ab_{93-98}, $FeO_T \leq 0.26$ wt% and $MgO \leq 0.08$ wt%, while rapakivi core are Or_{95-98}, $FeO_T \leq 0{,}32$ wt% and $MgO \leq 0.02$ wt%. At the rapakivi rim, Ba and Sr concentrations frequently range between 15 and 495 and 79–286 ppm, respectively. Plagioclase microphenocrysts enveloped by biotite have Ab_{96} and FeO_T contents ≤ 0.10 wt% and MgO below the detection limit and Sr and Ba contents of 249 – 134 ppm and 16–162 ppm, respectively.

In general, trace elements of plagioclase crystals define two groups (Fig. 4a–c). Both consist of phenocrysts and rapakivi crystals. Group 1 comprise plagioclases with Sr concentration ranging from 117 to 310 ppm, and Sr/Ba ratios ranging from 4 to 17. Group 2 has Sr/Ba ranging from 0 to 6 and Sr content from 53 to 148 ppm. Few data of microphenocrysts do not allow a clear determination of the trace elements groups. Results can be found in Table S2 in the ESM.

The REE content of the rapakivi plagioclase shows LREE normalized enrichment (La_N/Yb_N = 2.02-61.00) and Eu anomaly portraying very negative to high positive anomalies [Eu/Eu* = 0.35-5.00; with $Eu^*=(Sm \times Gd)^{0.5}$; Fig. 5]. The Th/U ratio is mostly between 1.35 and 5.78. The phenocrysts have more homogenous REE content than the rapakivi plagioclase, as well as less evident LREE enrichment (La_N/Yb_N = 0.18–25.24), negative to positive Eu anomalies (Eu/Eu* = 0.41–5.21), and Th/U ratio from 0.91 to 3.52.

Thermobarometry

Using Putirka (2008) approach temperature and pressure estimate, the Ab-An exchange coefficient represented by $K_D(An\text{-}Ab)^{pla-liq}$ was calculated using $T < 1050$ °C, 0.1 ± 0.05 and for $T > 1050$ °C, 0.28 ± 0.11. The acquired results do not correspond to the values specified by Putirka (2008), making the estimate of plagioclase temperature problematic.

In situ Sr isotopes

Sr isotopes in plagioclase from Contendas rhyolite highlight the presence of two populations; however, only one population accounts for almost all the crystals analyzed Fig. 6. Results can be found in Table S4 in the ESM. The $^{87}Sr/^{86}Sr$ ratios of all crystals have a wide range from 0.70700 to 0.70994 (Table 1). The phenocrysts exhibit moderate to high isotopic variations with $^{87}Sr/^{86}Sr_{core}$ (0.70762 and 0.70815) more radiogenic than the $^{87}Sr/^{86}Sr_{rim}$ (0.70704 and 0.70780). Meanwhile, the rims of rapakivi crystals show a bimodal distribution, 0.70700 and 0.70793. Some crystals show variations of $^{87}Sr/^{86}Sr_{core-rim}$ from high to moderate ratios ($\Delta^{87}Sr/^{86}Sr = 69.10^{-5}$, 53.10^{-5} and 35.10^{-5}), while other crystals show higher $^{87}Sr/^{86}Sr_{rim}$ values with moderate variation (0.70994 and 0.70946), Fig. 7.

Biotite

Biotite is found enveloping feldspars and quartz with sizes of 100–200 µm (Bt-1), and small skinny flakes with sizes < 50 µm (Bt-2) with some of them partly chloritized in the groundmass (Figs. 8 and 9). The structural formula of biotite was calculated following Li et al. (2020). Both biotite types indicate a Fe-rich nature in the $Al^{(vi)} + Fe^{3+} + Ti$ - Mg - Fe^{2+} + Mn diagram (Fig. 10a). In comparison to Bt-2, Bt-1 has higher FeO_T, TiO_2, and lower MgO. Bt-1 biotite has a

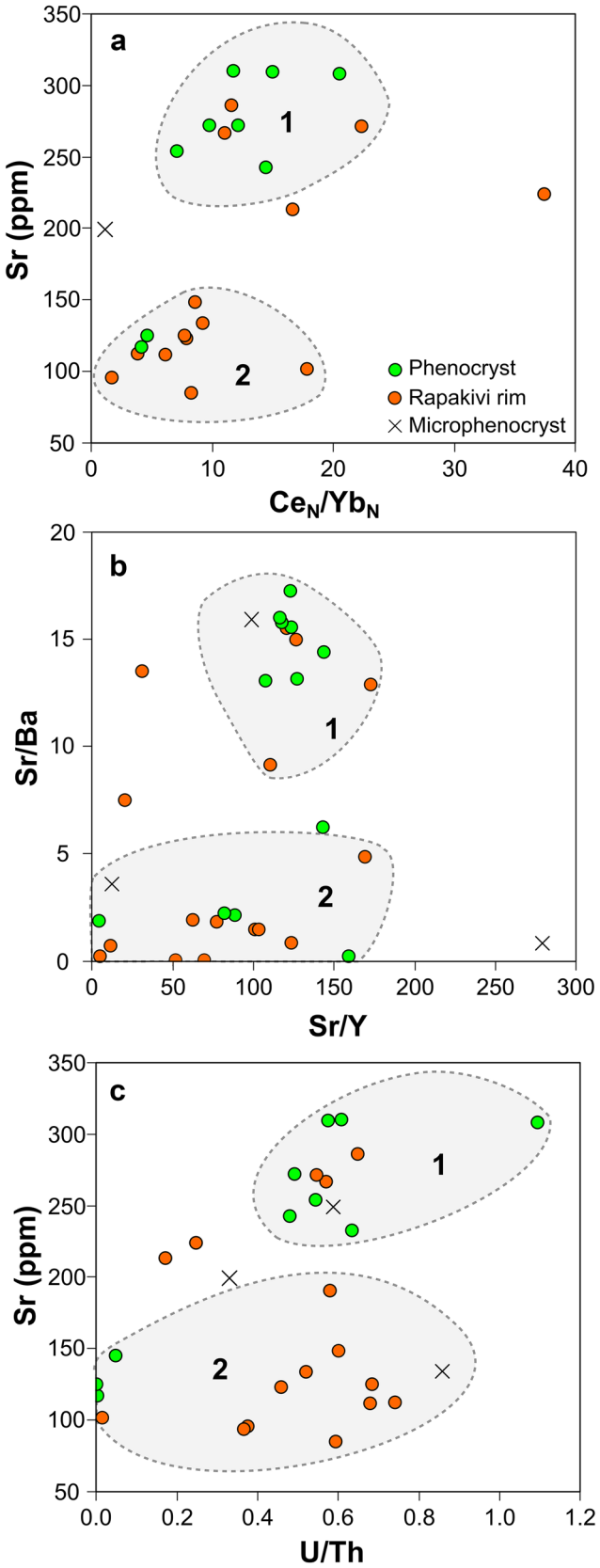

Fig. 4 Plots visualizing the chemical composition of feldspars from Contendas rhyolite. **a** Distribution of Sr versus Ce_N/Yb_N. **b** Sr/Ba versus Sr/Y. **c** Sr versus U/Yh in plagioclase crystals

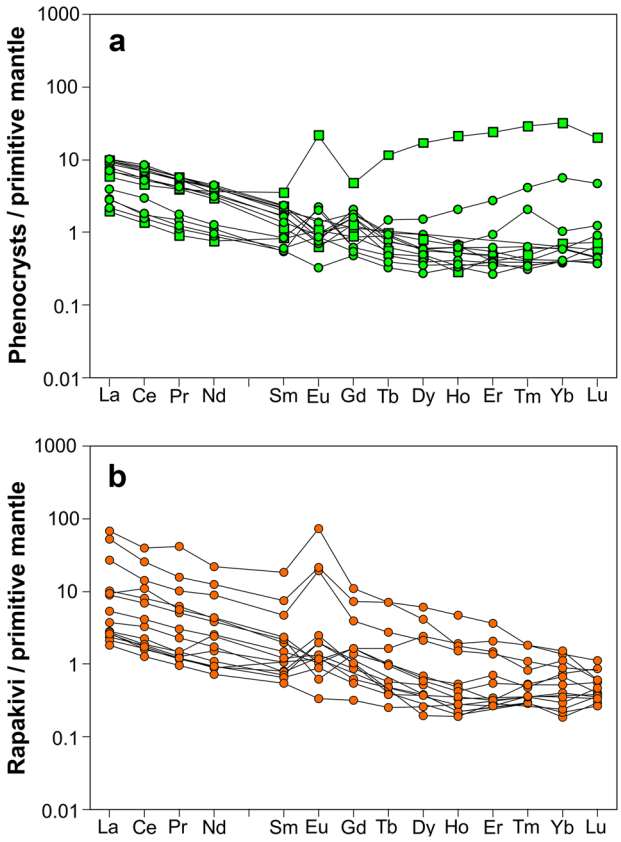

Fig. 5 Primitive mantle-normalized REE diagrams of plagioclases. Normalization values from McDonough and Sun (1995)

Fe/Fe + Mg ratio ranging from 0.75 to 0.79, whereas Bt-2 grains vary between 0.64 and 0.74.

Biotite Bt-2 can be distinguished into two sub-groups: Bt-2a, indicating MgO and TiO_2 contents from 4.59 to 5.31 wt% and 1.77–2.59 wt%; and Bt-2b, with MgO and TiO_2 ranging from 6.90 to 8.04 wt% and 0.99–1.56 wt%, respectively. Despite this, the Mg/(Mg + Fe) ratios in Bt-2 are higher (0.28–0.44) than in Bt-1 (0.25–0.28). The Al^T (1.35–1.55) of both biotites varies slightly, straddling the alkaline and peralkaline domains (Fig. 10b, c).

The chemistry of these different types of biotite has also revealed that the Bt-1 biotite and Bt-2a grains retain their primary composition while the Bt-2b grains are re-equilibrated (Table S3; Fig. 11a). The relationship among MgO-FeO-Al_2O_3 indicate an influence of anorogenic alkaline suites in a crustal nature (Fig. 11b, c). Another significant finding is the fO_2 of crystallization. The fO_2 estimates of Bt-1 and Bt-2 biotite using Fe^{2+}, Fe^{3+}, and Mg diagram of Wones and Eguster (1965) plot between the Ni-NiO and Fe_3O_4-Fe_2O_3 buffers (Fig. 11d).

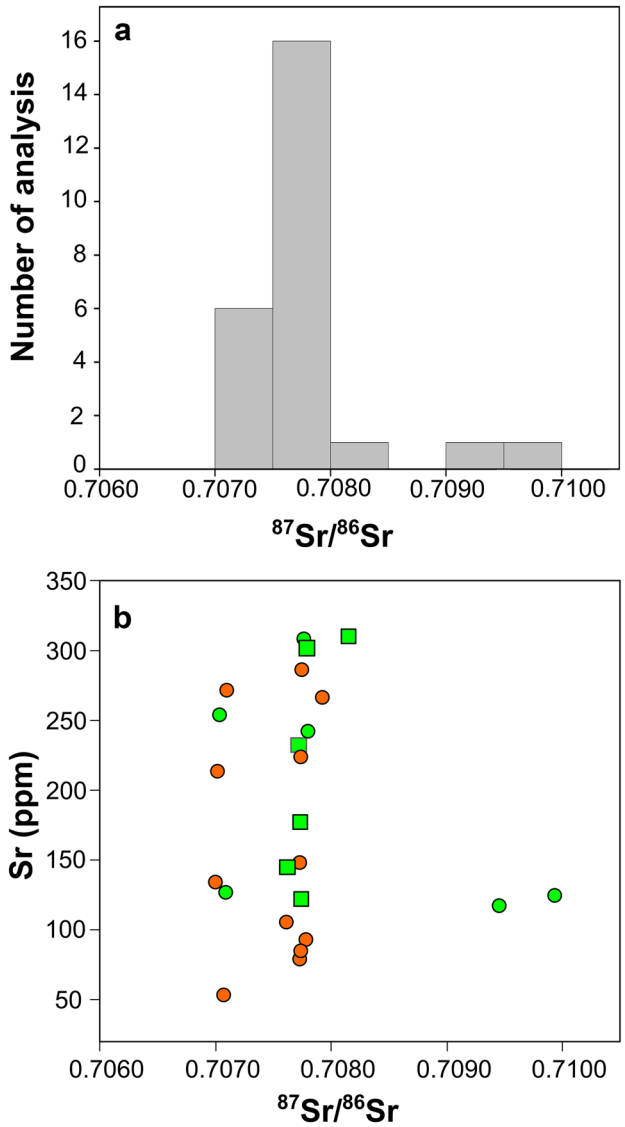

Fig. 6 **a** Histogram of Sr isotope composition of Contendas rhyolite plagioclase. **b** Plot of Sr concentrations versus $^{87}Sr/^{86}Sr$ ratios

Table 1 In-situ Sr isotope for plagioclase of Contendas rhyolite

Spot	Sample	Crystal	Spot zone	$^{87}Sr/^{86}Sr$	Error*
10	TZD-31 C	R	Rim	0.70702	0.00021
11			Rim	0.70793	0.00018
12			Rim	0.70710	0.00021
13			Rim	0.70789	0.00022
14			Rim	0.70775	0.00025
15			Rim	0.70774	0.00023
18	TZD-31 C	R	Rim	0.70773	0.00026
19	TZD-31 C	R	Rim	0.70762	0.00028
20			Rim	0.70779	0.00023
21			Rim	0.70707	0.00021
22	TZD-31 C	R	Rim	0.70773	0.00024
23			Rim	0.70700	0.00025
16	TZD-31E	R	Rim	0.70774	0.00022
29	TZD-31 C	P	Rim	0.70774	0.00015
24	TZD-31 C	P	Core	0.70772	0.00018
25	TZD-31E	P	Rim	0.70704	0.00022
26			Core	0.70773	0.0002
36	TZD-31E	P	Rim	0.70709	0.00021
38			Core	0.70762	0.00016
41	TZD-31E	P	Rim	0.70777	0.00016
40			Core	0.70779	0.00022
45	TZD-31E	P	Rim	0.70780	0.00017
43			Core	0.70815	0.00023
52	TZD-31D	P	Rim	0.70994	0.00035
53			Rim	0.70946	0.00036

R rapakivi, *P* phenocryst

*Errors are quoted at the 2s level

Discussion

Contendas rhyolite formed in a relatively shallow reservoir (< 10 km) as a result of the extraction of a felsic residual liquid (Zincone et al. 2016). According to the same authors, the high-silica rhyolite of ferroan affinity with signature of "A-type-like" composition generated from the cooling of granitic magmas, currently representing the remains of an eroded Paleoarchean volcanic-plutonic system in the São Francisco Craton.

Based on mineral scale chemistry fingerprints and petrographic features in this study, there is no evidence of distinct magmatic interactions of feldspars or biotite from the Contendas rhyolite, which could have influenced the composition and texture of minerals crystallized in the high-silica melt. The unusual geochemical features of this metasubvolcanic rock displayed composition similarities with Archean igneous rock from the Acasta Gneiss Complex (Zincone et al. 2016), whose genesis is linked to shallow-level magmatic processes and assimilation of rocks previously altered by surface waters (Reimink et al. 2014).

The Contendas rhyolite plagioclases are characterized by two important groups of crystals identified in the petrography: phenocrysts and rapakivi. Mineral scale investigation based mainly on the compositional variation of elements such as Sr, Ba, and LREE, record two groups of feldspars crystallization. Even though plagioclase has a negligible variation in the anorthite content, the variation in trace elements and Sr/Ba ratio may indicate the influence of distinct mechanisms or different stages of crystallization during plagioclase formation. Phenocrysts and rapakivi crystals are found in both groups, however phenocrysts predominate in group one, whereas rapakivi crystals, in the second. Given the inaccuracy of temperature-pressure of plagioclase estimation, the crystallization history is currently unknown,

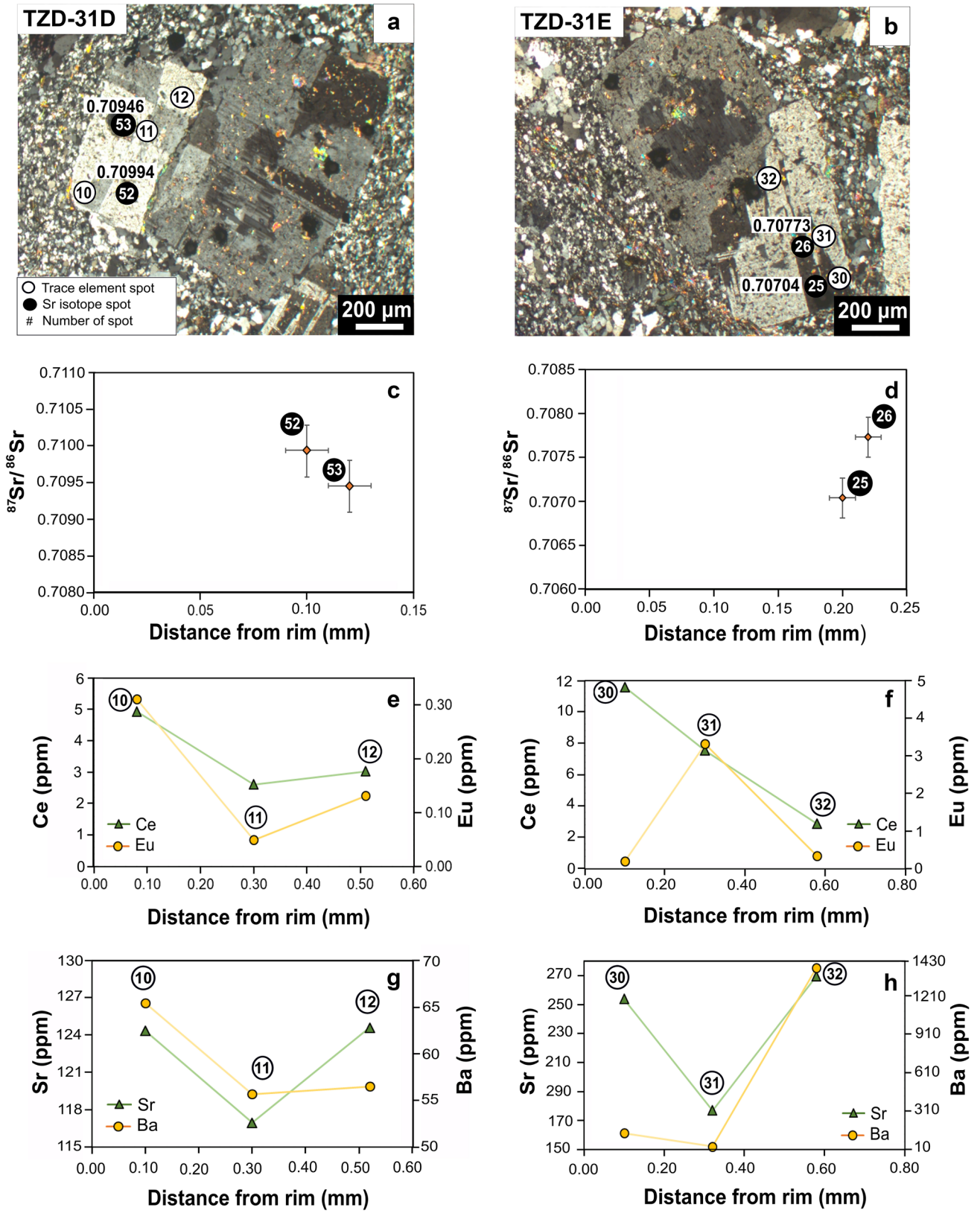

Fig. 7 Cross-polarised transmitted light images showing **a** tabular crystal of plagioclase clustered to a rapakivi and **b** plagioclase with irregular contact to a rapakivi. **c**, **d** Sr isotope composition according to the distance to rims of crystals. **e**, **f**, **g**, and **h** Distribution of Ce, Eu, Sr, and Ba according to the distance from rim

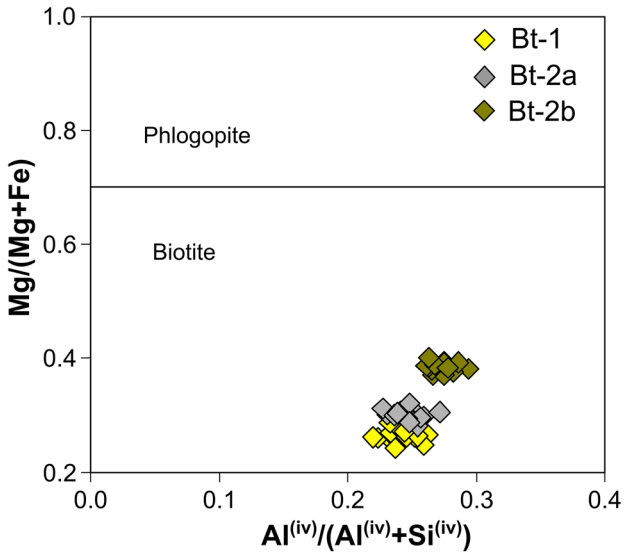

Fig. 8 Biotite composition of Contendas rhyolite in Mg/(Mg + Fe) versus $Al^{(iv)}/(Al^{(iv)} + Si^{(iv)})$ plot (after Deer et al. 1962)

particularly for an order of crystallization inferences. Phenocrysts and rapakivi from the first group contain more Sr and LREE than the second one, suggesting that the melt was enriched in LREE at the time of phenocrysts crystallization.

The bulk of phenocryst Sr isotopes show a slight Sr isotopic variation, with a low Sr isotope ratio near the rims compared to the cores, reflecting the influence of less radiogenic continental crust. The assimilation of less radiogenic country rock, rather than mixing interaction, was the most likely process driving differentiation. Moreover, the observed plagioclase demonstrated no significant variation in anorthite, despite the trace element heterogeneity. Another distinguishing chemical feature is the common negative Eu anomaly, whose partitioning is totally dependent on temperature and fO_2 (Weill 1973; Drake 1975). In the Contendas rhyolite, Eu and Sr were most likely removed from the melt through fractional crystallization of early plagioclase generation during intra-crustal differentiation.

Previous geochemical studies of the Contendas rhyolite recognized feldspars encased by biotite (e.g. Zincone et al. 2016), but due to the lack of sufficient data on this microstructure, it is too early to provide crystallization inferences. Despite this, petrographic evidences given by the size of the fine-grained feldspars encapsulated by biotite suggests a nucleation delay in the groundmass (e.g. Rusiecka and Martel 2022). Biotite crystals crystallized under iron-rich

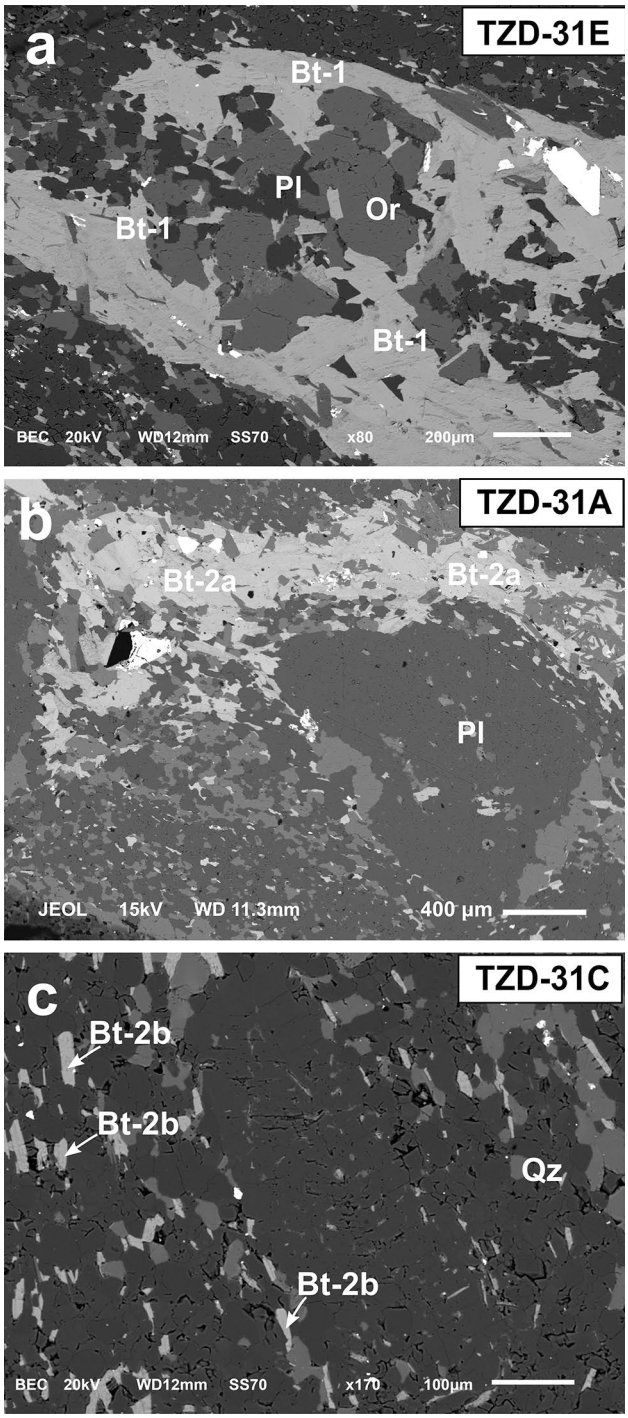

Fig. 9 Back-scattered electron images of **a** Bt-1 of sample TZD-31E, **b** Bt-2a of sample TZD-31 A and **c** Bt-2b of sample TZD-31Ce. Mineral abbreviations are: Bt – biotite; Or – orthoclase; Pl – plagioclase; Qz - quartz

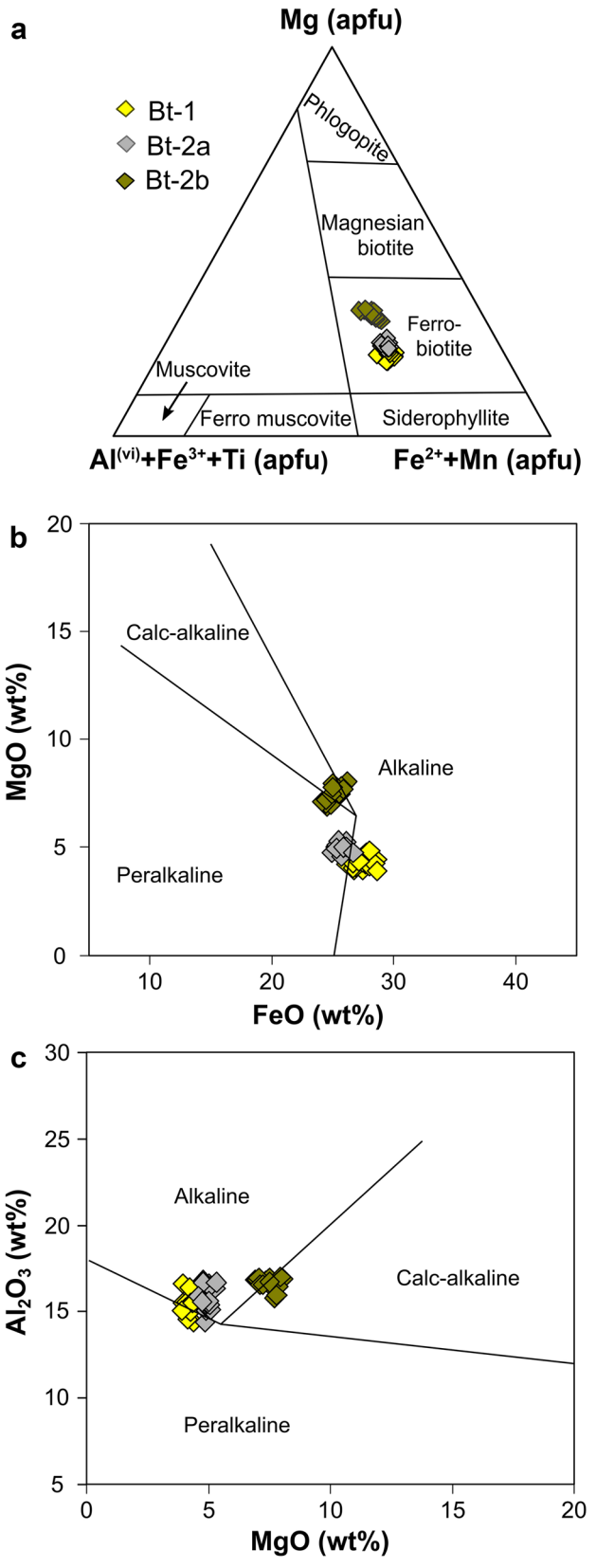

Fig. 10 Chemical compositions of biotite Bt-1, Bt-2a, and Bt-2b. **a** ▶ Ternary diagram $Al^{(iv)}+Fe^{3+}+Ti$-Mg-Fe^{2+}-Mn, showing the Fe-rich nature of samples (after Foster 1960). **b** Composition variation of MgO versus FeO and **c** Al_2O_3 versus MgO, depicting a magmatic source classification (after Abdel-Rahman and Abdel Fattah 1994)

environment and oxidized conditions (fO_2). The chemical signature of biotite crystals indicate an anarogenic source with a magmatic system generated from a continental crust, confirming earlier assumptions of Zincone et al. (2016) (Fig. 9c).

The negligible variation of the Sr isotope and the low Sr and LREE content in the rapakivi rims, indicate a magmatic scenario with low concentrations of these elements as plagioclase crystallization occurred in the magma. Furthermore, the irregular contact observed in rapakivi crystals between the K-feldspar core and the plagioclase rim suggests magmatic disequilibrium, most likely caused by changes in pressure and temperature. The shallow-level magmatism and the rising residual liquid could have reduced pressure and temperature conditions in the high-silica system, resulting in K-feldspar corrosion and the formation of plagioclase with patchy zoning (e.g. Vance 1965).

Glomerocrysts are common in the rhyolitic groundmass. They are composed of plagioclase, K-feldspar, and rapakivi crystals with planar and irregular internal contacts. The orientation of the aggregates and individual grains also suggests a magma flow. Previous paleomagnetism studies on the Contendas rhyolite revealed a coherent eastward sub-vertical lava flow direction during its formation (Amaral 2021). Such evidences indicate that aggregates formed during the turbulence of melt injection and ascent to the shallow reservoir (e.g. Turner and Campbell 1986). Cluster features, on the other hand, can be related to hydrodynamic forces in a magmatic flow through a process known as synneusis (e.g. Vance 1969). Vogt (1921) introduced this process and applied it to crystal segregation from magma at an early stage. This structure is commonly identified by the parallel relationship of the crystalline faces and the orientation of the twinning (Vance 1969). Despite this, the presence of rapakivi crystals in the clusters, reinforces the premise that individual feldspar crystals joined during the emplacement of the lava flow.

In this study, a detailed investigation from the mineral scale elucidates how a few magmatic mechanisms interacted and performed for the generation of distinctive plagioclase populations and primary biotite crystallization in high-silica magmatism. Although the thermobarometer investigation was restricted by mineral assemblage, the petrographic textures and chemical analyses highlight the primary aspects preserved in the mineral compositions of this unusual subvolcanic rock from the Contendas-Mirante region.

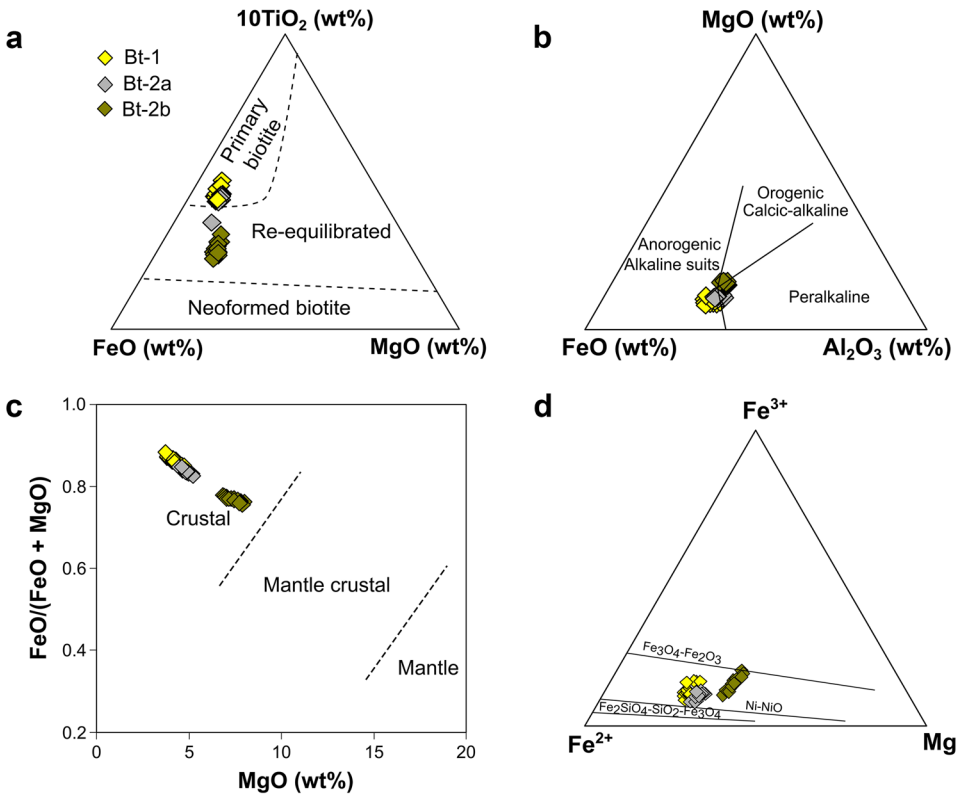

Fig. 11 **a** Ternary diagram FeO-10TiO_2-MgO indicating primary biotite for Bt-1 (after Nachit et al. 2005). **b** Ternary diagram FeO-MgO-Al_2O_3 depicting the magmatic nature of Bt-1, Bt-2a, and Bt-2b (after Abdel-Rahman and Abdel Fattah 1994). **c** FeO/(FeO + MgO) versus Mgo plot, showing the crustal nature of biotite (after Zhou 1986). **d** Fe^{2+}-Fe^{3+}-Mg ternary diagram of Bt-1, Bt-2a, and Bt-2b from Contendas rhyolite (after Wones and Eguster 1965). Fe_3O_4-Fe_2O_3 - hematite-magnetite; Ni-NiO - nickel-nickel oxide; Fe_2SiO_4-SiO_2-Fe_3O_4 - quartz-fayalite-magnetite

Conclusions

The Contendas subvolcanic rock is a meta-rhyolite with well-preserved petrographic and chemical igneous characteristics. The following are the main findings of this study: (i) The microstructures and chemical signatures of plagioclase populations reveal two main stages of generation. One stage indicates the crystallization of plagioclase phenocrysts and rapakivi with a high Sr/Ba content and slight LREE, while another stage records the crystallization of feldspars with low Sr/Ba. (ii) The small variations of plagioclase in-situ Sr isotope most likely point to subtle assimilation of country rock and highlight crystal evolution with no interactions from other processes such as magma mixing or mingling, constraining plagioclase populations and biotite formation to a continental crust composition. (iii) The chemical characteristics of primary biotite crystals indicate an anorogenic setting sourced by continental crust under oxidized conditions.

Supplementary Information The online version contains supplementary material available at https://doi.org/10.1007/s00710-023-00842-1.

Acknowledgements Author E.M.B.F wishes to thank the Fundação de Amparo à Pesquisa do Estado de Minas Gerais and Coordenação de Aperfeiçoamento de Pessoal de Nível Superior for providing a scholarship. We gratefully appreciate the assistance of the Microscopy and Microanalysis Laboratory, and the Isotopic Geochemistry Laboratory of Federal University of Ouro Preto, Minas Gerais State, Brazil. We are also grateful to three anonymous reviewers and the handling Editor Chao Wang for their thoughtful and constructive comments and suggestions that improved the quality of the manuscript.

Funding Author E.M.B.F was funded by Fundação de Amparo à Pesquisa do Estado de Minas Gerais and Coordenação de Aperfeiçoamento de Pessoal de Nível Superior. S. A. Z. received financial support from Ministério da Ciência, Tecnologia e Inovação and Conselho de Desenvolvimento Científico e Tecnológico (436648/2018), Fundação de Apoio a Pesquisa do Distrito Federal (193.001.263/2017), and Coordenação de Aperfeiçoamento de Pessoal de Nível Superior and Conselho de Desenvolvimento Científico e Tecnológico (465613/2014-4).

References

Abdel-Rahman, Abdel Fattah M (1994) Nature of biotites from alkaline, calc-alkaline, and peraluminous magmas. J Petrol 35:525–541

Agangi A, Hofmann A, Elburg MA (2018) A review of Palaeoarchaean felsic volcanism in the eastern Kaapvaal craton: linking plutonic and volcanic records. Geosci Front 9:667–688

Amaral CAD (2021) Paleomagnetic study of Bahia Archean rocks. Universidade de São Paulo

Barbosa JSF, Sabaté P (2004) Archean and Paleoproterozoic crust of the São Francisco Craton, Bahia, Brazil: geodynamic features. Precambrian Res 133:1–27

Barbosa JSF, Sabaté P, Marinho MM (2003) O cráton do São Francisco na Bahia: uma síntese. Rev Bras Geociências 33:3–6

Champion DC, Smithies RH (2007) Geochemistry of Paleoarchean Granites of the East Pilbara Terrane, Pilbara Craton, Western Australia: implications for early Archean Crustal Growth. Dev Precambrian Geol 15:369–409

Chen WT, Zhou MF, Gao JF, Zhao TP (2015) Oscillatory Sr isotopic signature in plagioclase megacrysts from the Damiao anorthosite complex, North China: implication for petrogenesis of massif-type anorthosite. Chem Geol 393–394:1–15

Condie KC (2019) Earth's Oldest Rocks and Minerals. Earth's Oldest Rocks. Elsevier B.V., pp 239–253

Deer WA, Howie RA, Zussman J (1962) Rock-forming minerals: sheet silicates, 3rd edn. Wiley

dos Santos C, Zincone SA, Queiroga GN et al (2022) Evidence for change in crust formation process during the Paleoarchean in the São Francisco Craton (Gavião Block): coupled zircon Lu-Hf and U-Pb isotopic analyses and tectonic implications. Precambrian Res 368:106472

Drake MJ (1975) Partition of Sr, Ba, ca, Eu2+ Y, Eu3+, and other REE between plagioclase feldspar and magmatic liquid: an experimental study. Geochim Cosmochim Acta 39:689–712

Foster MD (1960) Interpretation of the composition of trioctahedral micas. USGS Prof Pap 354:11–48

Gao JF, Zhou MF, Robinson PT et al (2015) Magma mixing recorded by Sr isotopes of plagioclase from dacites of the Quaternary Tengchong volcanic field, SE Tibetan Plateau. J Asian Earth Sci 98:1–17

Gordilho Barbosa R, Ferreira A, Leitzke FP et al (2022) A review of 3.66 to 2.77 Ga crustal differentiation in the northern São Francisco Craton, Brazil. Int Geol Rev 00:1–17

Griffin WJ, Powell J, Pearson NJ, O'Reilly SY (2008) Glitter: data reduction software for laser ablation ICP-MS. In: Sylvester P (ed) Laser ablation ICP-MS in the Earth Sciences: current Practices and Outstanding Issues, Mineralogi. Agilent Technologies, Vancouver, pp 308–311

Huston DL, Morant P, Pirajno F et al (2007) Paleoarchean mineral deposits of the Pilbara Craton: Genesis, tectonic environment and comparisons with younger deposits. In: Earth's Oldest Rocks. pp 411–450

Kemp AIS, Hawkesworth CJ, Foster GL et al (2007) Magmatic and crustal differentiation history of granitic rocks from Hf-O isotopes in zircon. Science (80-) 315:980–983

Kröner A, Elis Hoffmann J, Xie H et al (2013) Generation of early Archaean felsic greenstone volcanic rocks through crustal melting in the Kaapvaal, craton, southern Africa. Earth Planet Sci Lett 381:188–197

Laurent O, Martin H, Moyen JF, Doucelance R (2014) The diversity and evolution of late-archean granitoids: evidence for the onset of "modern-style" plate tectonics between 3.0 and 2.5 Ga. Lithos 205:208–235

Li X, Zhang C, Behrens H, Holtz F (2020) Corrigendum to "Calculating biotite formula from electron microprobe analysis data using a machine learning method based on principal components regression. Lithos 362–363. https://doi.org/10.1016/j.lithos.2020.105506

Marinho MM, Sabate P, Barbosa JSF (1993a) The Contendas-Mirante volcano-sedimentary belt. Bol IG-USP Publicação Espec 15:37–72

Marinho MM, Vidal P, Alibert C et al (1993b) Geochronology of the Jequié-Itabuna granulitic belt and of the Contendas-Mirante volcano-sedimentary belt. Bol IG-USP Publicação Espec 15:73–96

Martin H, Peucat JJ, Sabaté P, Cunha JC (1997) Crustal evolution in the early Archaean of South America: example of the Sete Voltas Massif, Bahia State, Brazil. Precambrian Res 82:35–62

Martin H, Smithies RH, Rapp R et al (2005) An overview of adakite, tonalite-trondhjemiten-granodiorite (TTG), and sanukitoid: Relationships and some implications for crustal evolution. Lithos 79:1–24

Mascarenhas JF, Ledru P, De Souza SL et al (1998) Geologia e recursos minerais do Grupo Jacobina e da parte sul do Greenstone Belt de Mundo Novo. Série Arq Abertos 13:58

McDonough WF, Sun SS (1995) The composition of the Earth. Chem Geol 120:223–253. https://doi.org/10.1016/0009-2541(94)00140-4

Nachit H, Ibhi A, Abia EH, Ben Ohoud M (2005) Discrimation between primary magmatic biotites, reequilibrated biotites and neoformed biotites. Comptes Rendus - Geosci 337:1415–1420

Nutman AP, Cordani UG (1993) SHRIMP U-Pb zircon geochronology of archaean granitoids from the Contendas-Mirante area of the São Francisco Craton, Bahia, Brazil. Precambrian Res 63:179–188

Oliveira EP, McNaughton NJ, Zincone SA, Talavera C (2020) Birthplace of the São Francisco Craton, Brazil: evidence from 3.60 to 3.64 Ga gneisses of the Mairi Gneiss Complex. Terra Nov 281–289. https://doi.org/10.1111/ter.12460

Putirka KD (2008) Thermometers and barometers for volcanic systems. Rev Mineral Geochem 69:61–120

Reimink JR, Chacko T, Stern RA, Heaman LM (2014) Earth's earliest evolved crust generated in an Iceland-like setting. Nat Geosci 7:529–533

Rusiecka MK, Martel C (2022) Nucleation delay in water-saturated rhyolite during decompression in shallow volcanic systems and its implications for ascent dynamics. Bull Volcanol 84:61

Sabaté P, Marinho MM, Vidal P, Caen-Vachette M (1990) The 2-Ga peraluminous magmatism of the Jacobina-Contendas Mirante belts (Bahia, Brazil): geologic and isotopic constraints on the sources. Chem Geol 83:325–338

Santos-Pinto M, Peucat J, Martin H et al (2012) Crustal evolution between 2.0 and 3.5 Ga in the southern Gavião block (Umburanas-Brumado-Aracatu region), São Francisco Craton, Brazil: a 3.5 e 3.8 Ga proto-crust in the Gavião block ? J South Am Sci 40:129–142

Smithies RH, Champion DC, Van Kranendonk MJ (2019) The oldest well-preserved felsic volcanic rocks on Earth: geochemical clues to the early evolution of the Pilbara Supergroup and implicationss for the growth of a Paleoarchean protocontinent. Earth's Oldest Rocks. Government of Western Australia and Elsevier, pp 463–486.

Teixeira W, Oliveira EP, Marques LS (2017) Nature and evolution of the Archean crust of the São Francisco Craton. In: Heibron M, Cordani UG, Alkimim FF (eds) The São Francisco Craton and its margins. Springer, pp 29–56

Teles G, Chemale F, de Oliveira CG (2015) Paleoarchean record of the detrital pyrite-bearing, Jacobina Au-U deposits, Bahia, Brazil. Precambrian Res 256:289–313

Tepley FJ, Davidson JP (2003) Mineral-scale Sr-isotope constraints on magma evolution and chamber dynamics in the rum layered intrusion, Scotland. Contrib to Mineral Petrol 145:628–641

Turner JS, Campbell IH (1986) Convection and mixing in magma chambers. Earth Sci Rev 23:255–352

Vance JA (1965) Zoning in Igneous Plagioclase: patchy zoning. J Geol 73:636–651

Vance JA (1969) On synneusis. Contrib to Mineral Petrol 24:7–29

Vogt JHL (1921) The physical chemistry of the crystallization and magmatic differentiation of igneous rocks. J Geol 29:318–350

Weill DF (1973) Europium anomaly in plagioclase feldspar: experimental results and semiquantitative model. Science (80-) 180:1059–1060

Whitney DL, Evans BW (2010) Abbreviations for names of rock-forming minerals. Am Mineral 95:185–187

Wilson SA (1997) Data compilation for USGS reference material BHVO-2, Hawaiian Basalt. US geological survey open-file report

Wolff JA, Ellis BS, Ramos FC (2011) Strontium isotopes and magma dynamics: insights from high temperature rhyolites. Geology 39:931–934

Wones DR, Eguster HP (1965) Stability of biotite: experiment, theory, and application. Am Mineral 50:1228–1272

Yang YH, Wu FY, Xie LW et al (2011) High-precision direct determination of the 87Sr/86Sr isotope ratio of bottled Sr-rich natural mineral drinking water using multiple collector inductively

coupled plasma mass spectrometry. Spectrochim Acta - Part B At Spectrosc 66:656–660
Zhou ZX (1986) The origin of intrusive mass in Fengshandong. Acta Petrol Sin 2:59–70
Zincone SA, Oliveira EP (2017) Field and geochronological evidence for origin of the Contendas-Mirante supracrustal Belt, São Francisco Craton, Brazil, as a paleoproterozoic foreland basin. Precambrian Res 299:117–131
Zincone SA, Oliveira EP, Laurent O et al (2016) 3.30 Ga high-silica intraplate volcanic–plutonic system of the Gavião Block, São Francisco Craton, Brazil: evidence of an intracontinental rift following the creation of insulating continental crust. Lithos 266–267:414–434